Nanoscale

Accepted Manuscript

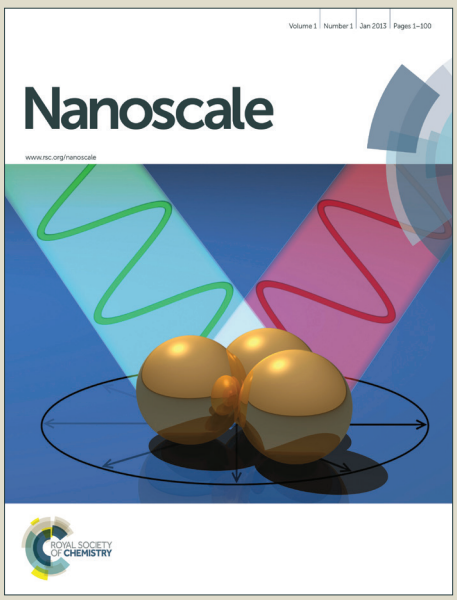

This is an *Accepted Manuscript*, which has been through the Royal Society of Chemistry peer review process and has been accepted for publication.

Accepted Manuscripts are published online shortly after acceptance, before technical editing, formatting and proof reading. Using this free service, authors can make their results available to the community, in citable form, before we publish the edited article. We will replace this *Accepted Manuscript* with the edited and formatted *Advance Article* as soon as it is available.

You can find more information about *Accepted Manuscripts* in the Information for Authors.

Please note that technical editing may introduce minor changes to the text and/or graphics, which may alter content. The journal's standard Terms & Conditions and the Ethical guidelines still apply. In no event shall the Royal Society of Chemistry be held responsible for any errors or omissions in this *Accepted Manuscript* or any consequences arising from the use of any information it contains.

ROYAL SOCIETY OF CHEMISTRY

www.rsc.org/nanoscale

One-Step Synthesis of Porous Bimetallic PtCu Nanocrystals with High Electrocatalytic Activity for Methanol Oxidation Reaction

Kamel Eid,[a,b] Hongjing Wang,[a] Pei He,[c] Kunmiao Wang,[c] Tansir Ahamad,[d] Saad M. Alshehri,[d] Yusuke Yamauchi,[d,e] and Liang Wang*[a]

[a] State Key Laboratory of Electroanalytical Chemistry, Changchun Institute of Applied Chemistry, Chinese Academy of Sciences, Changchun, Jilin 130022, P.R. China

[b] University of Chinese Academy of Sciences, Beijing 100039, P.R. China

[c] Key Laboratory of Tobacco Chemistry of Yunnan Province, China Tobacco Yunnan Industrial Co., Ltd., Kunming, Yunnan 650231, P.R. China

[d] Department of Chemistry, College of Science, King Saud University, Riyadh 11451, Saudi Arabia

[e] World Premier International (WPI) Research Center for Materials Nanoarchitectonics (MANA), National Institute for Materials Science (NIMS), 1-1 Namiki, Tsukuba, Ibaraki 305-0044, Japan

*Corresponding author's e-mail: wangliang@ciac.ac.cn

Nanoscale Accepted Manuscript

Abstract

The design of porous bimetallic nanocrystals (NCs) is very important for electrochemical energy conversions. Herein, we report an aqueous solution method for one-step fabrication of porous PtCu NCs assembled by spatially interconnected arms in high yield by a simple ultrasonic treatment of the reaction mixture at room temperature. The proposed method, without the need for multi-step synthesis, high temperatures, and organic solvents, shows an obvious advantage in its simplicity for the feasible synthesis of bimetallic PtCu NCs with a porous structure. As-made porous PtCu NCs are highly active and durable catalysts for a methanol oxidation reaction benefited from its porous structure and bimetallic composition.

Nanoscale Accepted Manuscript

1. Introduction

The direct methanol fuel cell (DMFC) is a very promising renewable energy source due to its high energy density.[1-4] The commercial development of DMFC is hindered by the high cost and low abundance of Pt material.[5] One of the most effective strategies to solve this problem is to alloy Pt with non-noble metals such as Co, Ni, Fe, and Rh.[6-9] This strategy can greatly improve the utilization efficiency of the very rare and expensive Pt and greatly enhance its catalytic activity and durability, ascribed to the favorable composition effect.[6-9]

Among various Pt-based bimetallic materials, PtCu nanocrystals (NCs) are particularly interesting catalysts, primarily due to their favorable electronic effect derived from the bimetallic Pt and Cu compositions.[10-14] This favorable electronic effect downshifts the *d*-band center of Pt, leading to the suppression of Pt oxides.[10-15] In addition to their composition, controlling the structure of PtCu NCs can further enhance their catalytic activity. PtCu NCs with different shapes, such as spheres, bipyramids, octahedrons, and cubes, have been demonstrated.[10-15] For example, PtCu nanosheets and nanocones are prepared by a two-step method using preformed gel-like material to confine the nucleation and subsequent growth of the nanocrystals, and PtCu nanorods are synthesized in a mixed solvent containing oleic acid, oleylamine, and 1-octadecene at 225°C for 30 min.[16-18] The reported synthetic approaches usually perform in boiling-point organic solvents at high temperatures.

Porous PtCu NCs are very promising catalysts due to their higher surface area relative to their solid counterparts.[19] A few porous PtCu NCs, such as cages and frames, have been prepared for catalytic applications. [20-23] For instance, PtCu nanoframes, which are synthesized by using ethylene glycol as a solvent at 140ºC for 90 min, are active catalysts for formic acid oxidation; and PtCu nanocages, which are prepared by using oleylamine as a solvent at 170°C for 24 h, are efficient catalysts for methanol oxidation reaction (MOR).[24,25] Despite advances in the synthesis of porous PtCu NCs, the reported syntheses generally rely on multi-step procedures, high temperatures, and organic

Nanoscale Accepted Manuscript

solvents.[10-15, 20-25] The development of a facile method in aqueous solution at room temperature to efficiently prepare porous bimetallic PtCu catalysts remains a great challenge.

Herein, we propose a one-step solution-phase method for direct synthesis of PtCu NCs with porous interiors and exteriors, which is simply performed by ultrasonic treatment of an aqueous solution containing K_2PtCl_4, $CuCl_2.6H_2O$, poly(vinylpyrrolidone) (PVP), and ascorbic acid (AA) for 15 min at room temperature. The developed method greatly simplifies the synthetic procedures, making it highly feasible. As-made porous PtCu NCs with spatially and locally separated arms are highly active catalysts for MOR.

2. Experimental section

Materials. K_2PtCl_4, $CuCl_2 \cdot 6H_2O$, L-ascorbic acid, poly(vinylpyrrolidone) (MW = 40,000), and methanol were purchased from Beijing Chemical Reagent (Beijing, China). A commercial Pt/C catalyst was ordered from Alfa Aesar.

Synthesis of porous PtCu NCs. Porous PtCu NCs were typically synthesized by using 1 mL of aqueous solution containing 0.3 mL of 20 mM $CuCl_2.6H_2O$, 0.7 mL of 20 mM K_2PtCl_4, and 0.01 g of PVP in which 1 mL of 0.1 M AA was quickly added, and then the mixture was sonicated for 15 min at room temperature. The product was collected by centrifugation at 10,000 rpm for 20 min, followed by three consecutive washing/centrifugation cycles with water, and then kept for further characterization.

Characterizations. The particle size and morphology were investigated using a Hitachi H-8100 EM transmission electron microscope (TEM) with an accelerating voltage of 100 kV, and a JEM-2010 operating at 200 kV equipped with energy dispersive spectrometer (EDS) analyses. X-ray diffraction (XRD) was recorded on a D8 ADVANCE (Bruker AXS, Germany) diffractometer equipped with Cu Kα radiation. The nitrogen physisorption isotherms were measured on a Quantachrome Autosorb 3.01 instrument, and samples were degassed for 24 h at 50ºC under vacuum before the measurements. The inductively coupled plasma optical emission spectrometry (ICP-OES) analysis was conducted using a

Nanoscale Accepted Manuscript

Thermo Scientific iCAP6300 (Thermo Fisher Scientific, US). X-ray photoelectron spectroscopy (XPS) analysis was performed using an ESCALAB MK II spectrometer (VG Scientific, UK) with Al Kα X-ray radiation for excitation.

Electrochemical investigations. Cyclic voltammogram (CV) experiments were performed using a CHI 832C electrochemical analyzer (Chenhua Co., Shanghai, China). A conventional three-electrode cell was used, including a Ag/AgCl (saturated KCl) electrode as a reference electrode, a Pt wire as a counter electrode, and a working electrode. The working electrode was a modified glassy carbon electrode (GCE) (3 mm in diameter) coated with different catalysts with the same loading amount of 10 μg and dried at room temperature. Then 3 μL of Nafion (0.05%) was coated on the surface of the modified GCE and dried before electrochemical experiments. MOR measurements were performed in a 0.1 M N_2-saturated $HClO_4$ solution containing 1 M methanol at a scan rate of 50 mV s^{-1}. MOR durability tests were performed at 0.6 V with a scan rate of 50 mV s^{-1} with cycles from 0 to 2,000. Current densities were normalized in reference to the geometric area of the working electrode, and specific and mass activities were normalized in reference to the electrochemical surface areas (ECSAs) and loading amount of Pt, respectively. The ECSAs were calculated by the following equation: ECSA = $Q_H / m \times 210$, where Q_H is the charge for H_{upd} adsorption determined using $Q_H = 0.5 \times Q$ (where Q is the charge in the H_{upd} adsorption–desorption area obtained after the double layer correction region between 0 and 0.37 V), m is the Pt loading amount on the electrode, and 210 μC cm^{-2} is the charge required for the monolayer adsorption of hydrogen on the Pt surface.

3. Results and discussion

Porous PtCu NCs are prepared by a one-step solution-phase reaction without the need for high temperature and organic solvent. **Figure 1a** reveals that the PtCu NCs are well-dispersed nanoparticles with a narrow size distribution ranging from 12 to 20 nm in a high yield. The average diameter is around 15 nm (**Figure S1a**). The PtCu NCs are assembled by spatially interconnected arms, with an

Nanoscale Accepted Manuscript

average diameter of 3 nm, that make pores in the exteriors and interiors of each nanoparticle (**Figure 1b**). XPS analysis of the NCs shows the presence of Pt and Cu elements (**Figure S2**). Elemental mapping images and cross-sectional compositional line profiles reveal that the PtCu NCs are alloyed structures (**Figure 2 and Figure S3 a,b**). The atomic ratio of Pt/Cu is 3/1, which is confirmed by ICP-OES and EDS analysis. Formation of the PtCu NC alloyed structure is further confirmed by XRD analysis (**Figure S4**). The characteristic peaks in the XRD pattern of the porous PtCu NCs are indexed as a typical metallic face-centered cubic (*fcc*) structure. There are no peaks for a single component of Pt or Cu in the XRD pattern, suggesting the purity of the single-phase PtCu alloy. This XRD pattern is consistent with those of previously reported alloyed PtCu nanoframes, PtCu nanocages, and PtCu nanocubes.[22–25] The lattice fringes of the porous PtCu NCs are extended across the arms without obvious phase segregation, indicating the well mixing of Pt and Cu atoms (**Figure 3a**). This implies that the formation of porous PtCu NCs is from nucleation and subsequent growth rather than from random particle aggregation. Fourier filtered lattice fringe images of one nanoparticle are mainly assignable to {111}, {110}, and {100} facets for the core area and {200}, {220}, and {311} facets for the shell region (**Figure 3b, c**).

To explore the formation mechanism of the porous PtCu NCs, monometallic Pt NCs and Cu NCs are prepared under the typical synthetic conditions. The synthetic processes can be visibly monitored via the evolution of the reaction solution color, which is time dependent over the course of the reaction. In the case of using a single Pt precursor, the color of the reaction solution changes from transparent, light brownish yellow to brown, then changes to opaque black within 15 min, and Pt NCs with a dendritic shape are obtained (**Figure S5a**). When a single Cu precursor is used, the reaction solution color changes from blue to deep yellow after 4 h, implying that it is difficult for AA to completely reduce Cu ions, and only irregular nanoparticles are obtained (**Figure S5b**). The complete reduction of Cu ions should result in a brownish red color. This is ascribed to the difference of reductive capability of AA for Pt and Cu precursors based on the reduction potentials of $PtCl_4^{2-}$/Pt

Nanoscale Accepted Manuscript

(0.755 V *vs.* RHE) and Cu^{2+}/Cu (0.340 V *vs.* RHE).[22] When both metallic Pt and Cu precursors are used in bimetallic synthesis, the solution color immediately changes from yellow to black, indicating the more rapid reduction rate of Pt with Cu relative to the single Cu system attributed to the autocatalytic effect.[22] In addition, when the synthesis process is carried out without PVP, the obtained PtCu NCs show solid interiors and smooth exteriors without any porous structural feature, indicating that PVP plays the dual roles of a capping agent and a structure-directing agent (**Figure S6**).

On the basis of these results, it can be speculated that the Pt nuclei are initially and rapidly produced, and then the Pt nuclei stimulate reduction of the Cu precursor. This results in the simultaneous co-reduction to form PtCu NCs. During the particle growth, PVP molecules adsorb onto the particle surfaces with the carbonyl group and pyrrolidone ring.[26] This causes anisotropic particle growth during the addition of atoms, which favors the formation of the branched structure with a porous structural feature.[27-31] Additionally, the ultrasonic irradiation effect plays an important role in the formation of porous PtCu NCs. In contrast, the ultrasonic treatment is replaced by a magnetic stirring treatment for single metal (Pt and Cu) and bimetal (PtCu) systems. Under a magnetic stirring treatment, the reaction solution color changes from transparent light brownish yellow to black after 1 h for a single Pt precursor; no reaction color change is observed for a single Cu reagent, even after 24 h; and Pt with a Cu precursor reaction solution color changes after 2 h. It is obvious that the reduction rate of metallic precursors is dramatically accelerated by the ultrasound radiation in comparison with the magnetic stirring treatment. The use of ultrasonic irradiation has been demonstrated to be a powerful strategy for the preparation of metallic NCs with porous structures.[32-34] The ultrasonically induced reduction benefits from the effect of acoustic cavitation. Vacuum bubbles are acutely formed and implosively collapsed in solution, which generates a transient high temperature and pressure as well as strong stirring power.[32–34] Consequently, the reduction reaction is greatly accelerated. Under the magnetic stirring treatment, dendritic PtCu NCs assembled by staggered arms are obtained (Here we define PtCu NCs with less porosity as dendritic PtCu NCs.) (**Figure 4**). The particle size narrowly

Nanoscale Accepted Manuscript

ranged from 16 to 26 nm, with a dominating diameter of 22 nm (**Figure S1b**). XPS analysis shows that the NCs include Pt and Cu elements (**Figure S2**). Cross-sectional compositional line profiles show that the dendritic PtCu NCs are in an alloyed form (**Figure S3c,d**). The atomic ratio of Pt/Cu is 9/1 as tested by ICP-OES and EDS analysis. Appropriate reducing kinetics is critical for the formation of porous PtCu NCs. The attempt to replace AA with sodium borohydride as a reducing agent in the typical synthesis leads to a bulk precipitate because of that the reduction process is too fast.

N_2 adsorption-desorption analysis shows that the porous PtCu NCs have a high surface area of 54.2 m^2 g^{-1}, and the pore diameters are calculated to be around 2.5 nm, ascribed to their porosity throughout the nanoparticles (**Figure 1** and **Figure 5a,b**). Dendritic PtCu NCs exhibit a lower surface area of 23.7 m^2 g^{-1} and obscure pores due to the lack of obvious porosity in their interiors (**Figure 4** and **Figure 5c,d**). Creating porous cavities in each PtCu NC helps dramatically increase its surface area. The ultrasonically induced reduction is highly favorable for the synthesis of porous PtCu NCs with a high molecular accessibility, which consequently favors the utilization efficiency of Pt. It is noted that the obtained surface area of porous PtCu NCs (54.2 m^2 g^{-1}) is higher than those of the reported PtPd nanocages (53 m^2 g^{-1}), mesoporous Pd@Pt NCs (40 m^2 g^{-1}), and Pt nanoballs (23 m^2 g^{-1}).[35-37]

Methods for the synthesis of PtCu NCs with different shapes have been previously reported.[10-25] For example, PtCu nanocubes are made by using 1-octadecene as a solvent containing tetraoctylammonium bromide and oleylamine at 230°C for 20 min, which is subsequently quenched by injecting toluene.[23] The previously reported methods are difficult to scale up because they are performed at high temperatures in organic solvents.[10-25] The proposed route is highly feasible for the synthesis of porous PtCu NCs with a uniform size and a high surface area (54.2 m^2 g^{-1}) in a high yield at room temperature in aqueous solution. These features are highly favorable for the preparation catalysts for catalytic applications.

Inspired by its attractive porous bimetallic architecture, the porous PtCu NCs are tested as promising catalyst for MOR, and its electrocatalytic activity is benchmarked against dendritic PtCu

Nanoscale Accepted Manuscript

NCs and a commercially available Pt/C catalyst. The active ECSA of porous PtCu NCs (54.1 $m^2 g^{-1}$) is 1.5 times higher than that of dendritic PtCu NCs (35.2 $m^2 g^{-1}$) and 1.1 times higher than that of Pt/C (50.6 $m^2 g^{-1}$) due to its richness in pores (**Figure S7**). **Figure 6a** shows the CVs of MOR catalyzed by the three catalysts measured in a 0.1 M $HClO_4$ aqueous solution with 1 M CH_3OH at room temperature. The current density of porous PtCu NCs in the positive direction sweep (13.01 mA cm^{-2}) is about 1.7 times higher than that of dendritic PtCu NCs (7.57 mA cm^{-2}) and 3.5 times higher than that of Pt/C (3.7 mA cm^{-2}). The ratio of I_f to I_b (the forward and backward current densities, respectively) is an important indicator for evaluation of the poison tolerance of the catalyst.[8] The I_f/I_b ratio of porous PtCu NCs (2.43) is higher than those of dendritic PtCu NCs (1.7) and Pt/C (1.21), implying its superior CO poison tolerance. **Figure 6b** displays the comparisons of mass activities and specific activities of the three tested catalysts. The MOR activity of porous PtCu NCs is better than that of dendritic PtCu NCs and Pt/C in terms of both mass activity and specific activity. The mass activity of porous PtCu NCs (1.55 mA μg^{-1}_{Pt}) is 3.9 times higher than that of dendritic PtCu NCs (0.4 mA μg^{-1}_{Pt}) and 10.5 times higher than that of Pt/C (0.148 mA μg^{-1}_{Pt}). The specific activity for porous PtCu NCs (2.88 mA cm^{-2}) is also obviously higher than that of the dendritic PtCu NCs (1.14 mA cm^{-2}) and Pt/C (0.293 mA cm^{-2}). The mass activity of the as-made porous PtCu NCs is superior to that of previously reported PdPt nanocages (0.58 mA μg^{-1}_{Pt}), PtCu nanodendrites (0.35 mA μg^{-1}_{Pt}), $Au/Cu_{64}Pt_{36}$ NCs (0.44 mA μg^{-1}_{Pt}), and mesoporous PtRu NCs (0.384 mA μg^{-1}_{Pt}).[35,22,38,41] The durability is important for a catalyst in MOR. After 2,000 cycles, the current densities of the porous PtCu NCs, dendritic PtCu NCs, and Pt/C keep a reservation of 95%, 84%, and 65% relative to their initial current densities, respectively, indicating the better durability for MOR of porous PtCu NCs than the two referenced materials (**Figure 7a-c**). The excellent durability of the porous PtCu NCs for MOR is attributed to its stable active surface. The shape of the porous PtCu NCs is reserved after the durability test (**Figure S8**). The porous PtCu NCs retain 94.5% of their initial ECSA, while dendritic PtCu NCs and Pt/C reserve 82% and 74%, respectively, after 2,000 cycle tests (**Figure 7d**).

Nanoscale Accepted Manuscript

Considering their porous and bimetallic structural features, the enhanced activity of porous PtCu NCs is attributed to the effect of their structure and composition.[10-14,39-41] The porous PtCu NC is an inherent three-dimensional, self-supported architecture that affords sufficient accessible active sites from both interiors and exteriors of the particles and improves the stability of active sites against undesirable particle agglomeration.[8,22-25] The porous structure is much more favorable for a catalyst than dendritic structure which only provides active sites from exterior surfaces. The bimetallic composition endows the synergy effect on the catalytic property. The Pt electronic binding energy is lowered by alloying with Cu due to the strong lattice contracts between Pt and Cu, facilitating cleavage of the C-H bond in MOR. The presence of Cu promotes the production of oxygenated species required for methanol oxidation to CO_2 *via* $HCOO^-$ intermediates instead of CO, making the material not susceptible to undesirable CO poison.[10-14,42,43] The catalytic performance of the porous PtCu NCs with an atomic Pt/Cu ratio of 3/1 is higher than that of the dendritic PtCu NCs with an atomic Pt/Cu ratio of 9/1. Besides its favorable porous structure, the enhanced activity of the porous PtCu NCs is partly ascribed to its richer Cu content.[44]

4. Conclusion

In summary, we have developed a solution-phase method for the one-step synthesis of porous PtCu NCs by an ultrasonic treatment of the aqueous reaction mixture at room temperature. The proposed method is much simpler relative to the reported thermal decomposition routes with high-boiling-point organic solvents. As-made porous PtCu NCs with spatially interconnected arms are highly active and durable catalysts for MOR, benefiting from their porous porous structure and bimetallic composition. This efficient approach is highly favorable for the facile synthesis of porous bimetallic electrocatalysts for electrochemical applications.

Nanoscale Accepted Manuscript

Acknowledgments

This work was supported by the National Natural Science Foundation of China (No. 21273218). K. Eid greatly appreciates the CAS-TWAS President's Fellowship. The authors extend their sincere appreciation to the Deanship of Scientific Research at King Saud University for funding this Prolific Research Group (PRG-1436-19).

Nanoscale Accepted Manuscript

References

1 S. Guo, S. Zhang and S. Sun, *Angew. Chem. Int. Ed.,* 2013, **52**, 8526-8544.

2 C. Li, T. Sato and Y. Yamauchi, *Angew. Chem. Int. Ed.,* 2013, **52**, 8050-8053.

3 G. Zhang, Z. Yang, C. Huang, W. Zhanga and Y. Wang, *Nanoscale*, 2015, **7**, 10170-10177.

4 H. Zhang, M. Jin and Y. Xia, *Chem. Soc. Rev*., 2012, **41**, 8035-8049.

5 M. K. Debe, *Nature,* 2012, **486**, 43-51.

6 A. Oh, H. Baik, D. S. Choi, J. Y. Cheon, B. Kim, H. Kim, S. J. Kwon, S. H. Joo, Y. Jung and K. Lee, *ACS Nano*, 2015, **9**, 2856-2867.

7 Y. Yu, W. Yang, X. Sun, W. Zhu, X.-Z. Li, D. J. Sellmyer and S. Sun, *Nano Lett*., 2014, **14**, 2778-2782.

8 Y. Zhang, M. Janyasupab, C.-W. Liu, X. Li, J. Xu and C.-C Liu, *Adv. Funct. Mater*., 2012, **22**, 3570-3575.

9 K. Eid, V. Malgras, P. He, K. Wang, A. Aldalbahi, S. M. Alshehri, Y. Yamauchi and L. Wang, *RSC Adv.,* 2015, **5**, 31147-31152.

10 F. Nosheen, Z.-C. Zhang, J. Zhuang and X. Wang, *Nanoscale*, 2013, **5**, 3660-3663.

11 J. Zhang, H. Yang, B. Martens, Z. Luo, D. Xu, Y. Wang, S. Zou and J. Fang, *Chem. Sci*., 2012, **3**, 3302-3306.

12 I. Mintsouli, J. Georgieva, S. Armyanov, E. Valova, G. Avdeev, A. Hubin, O. Steenhaut, J. Dille, D. Tsiplakides, S. Balomenou and S. Sotiropoulos, *Appl. Catal. B*, 2013, **136**, 160-167.

13 E. Taylor, S. Chen, J. Tao, L. Wu, Y. Zhu and *J.* Chen, *ChemSusChem.,* 2013, **6**, 1863-1867.

14 J. Zhang, J. Ma, Y. Wan, J. Jiang and X. S. Zhao, *Mater. Chem. Phys.,* 2012, **132**, 244-247.

15 W. Sang, T. Zheng, Y. Wang, X. Li, X. Zhao, J. Zeng and J. G. Hou, *Nano Lett*., 2014, **14**, 6666-6671.

16 F. Saleem, B. Xu, B. Ni, H. Liu, F. Nosheen, H. Li and X. Wang, Adv. *Mater*., 2015, **27**, 2013-2018.

17 F. Saleem, Z. Zhang, B. Xu, X. Xu, P. He and X. Wang, *J. Am. Chem. Soc.,* 2013, **135**, 18304-18307.

18 Q. Liu, Z. Yan, N. L. Henderson, J. C. Bauer, D. W. Goodman, J. D. Batteas and R. E. Schaak, *J. Am. Chem. Soc*., 2009, **131**, 5720-5721.

19 Y. Xu and B. Zhang, *Chem. Soc. Rev*., 2014, **43**, 2439-2450.

20 X. Yu, D. Wang, Q. Peng and Y. Li, *Chem. Commun*., 2011, **47**, 8094-8096.

21 Y. Jia, Y. Jiang, J. Zhang, L. Zhang, Q. Chen, Z. Xie and L. Zheng, *J. Am. Chem. Soc*., 2014, **136**,

Nanoscale Accepted Manuscript

3748-3751.

22 M. Gong, G. Fu, Y. Chen, Y. Tang and T. Lu, *ACS Appl. Mater. Interfaces,* 2014, **6**, 7301-7308.

23 D. Xu, Z. Liu, H. Yang, Q. Liu, J. Zhang, J. Fang, S. Zou and K. Sun, *Angew. Chem. Int. Ed*., 2009, **48**, 4217-4221.

24 S. Chen, H. Su, Y. Wang, W. Wu and J. Zeng, *Angew. Chem. Int. Ed.,* 2015, **54**, 108-113.

25 B. Y. Xia, H. B. Wu, X. Wang and X. W. Lou, *J. Am. Chem. Soc*., 2012, **134**, 13934-13937.

26 Y. Hu, P. Wu, H. Zhang and C. Cai, *Electrochim. Acta*, 2012, **85**, 314-321.

27 B. A. Kakade, T. Tamaki, H. Ohashi and T. Yamaguchi, *J. Phys. Chem. C,* 2012, **116**, 7464-7470.

28 B. Lim, M. Jiang, P. H.C. Camargo, E. C. Cho, J. Tao, X. Lu, Y. Zhu and Y. Xia, *Science,* 2009, **324**, 1302-1305.

29 K. Eid, H. Wang, V. Malgras, Z. A. Alothman, Y. Yamauchi and L. Wang, *J. Phys. Chem. C*, 2015, DOI: 10.1021/acs.jpcc.5b05867.

30 L. Wang and Y. Yamauchi, Chem. *Mater*., 2011, **23**, 2457-2465.

31 L. Wang and Y. Yamauchi, *Chem. Mater*., 2009, **21***,* 3562-3569.

32 J.-H. Jang, J. Kim, Y.-H. Lee, I. Y. Kim, M.-H. Park, C.-W. Yang, S.-J. Hwang and Y.-U. Kwon, *Energy Environ. Sci*., 2011, **4**, 4947-4953.

33 L. Wang and Y. Yamauchi, *J. Am. Chem. Soc.,* 2009, **131**, 9152-9153.

34 H. Ataee-Esfahani, L. Wang, Y. Nemoto and Y. Yamauchi, *Chem. Mater.,* 2010, **22**, 6310-6318.

35 L. Wang and Y. Yamauchi, *J. Am. Chem. Soc*., 2013, **135**, 16762-16765.

36 H. Ataee-Esfahani, M. Imura and Y. Yamauchi, *Angew. Chem. Int. Ed*., 2013, **52**, 13611-13615.

37 G. Surendran, L. Ramos, B. Pansu, E. Prouzet, P. Beaunier, F. Audonnet and H. Remita, *Chem. Mater.,* 2007, **19**, 5045-5048.

38 X. Sun, D. Li, Y. Ding, W. Zhu, S. Guo, Z. L. Wang and S. Sun, *J. Am. Chem. Soc.,* 2014, **136**, 5745-5749.

39 M. A. Mahmoud, R. Narayanan and M. A. El-Sayed. *Acc. Chem. Res*., 2013, **46**, 1795-1805.

40 P. Strasser, S. Koh, T. Anniyev, J. Greeley, K. More, C. Yu, Z. Liu, S. Kaya, D. Nordlund, H. Ogasawara, M. F. Toney and A. Nilsson, *Nat. Chem*., 2010, **2**, 454-460.

41 H. Ataee-Esfahani, J. Liu, M. Hu, N. Miyamoto, S. Tominaka, K. C. W. Wu and Y. Yamauchi, *Small*, 2013, **9**, 1047-1051.

42 A. V. Miller, V. V. Kaichev, I. P. P. Prosvirin and V. I. Bukhtiyarov, *J. Phys. Chem. C,* 2013, **117**, 8189-8197.

43 A. Mahata, I. Choudhuri and B. Pathak, *Nanoscale,* 2015, **7**, 13438-13451.

44 W. Hong, C. Shang, J. Wang and E. Wang, *Nanoscale*, 2015, **7**, 9985-9989.

Nanoscale Accepted Manuscript

Figures and Figure Captions

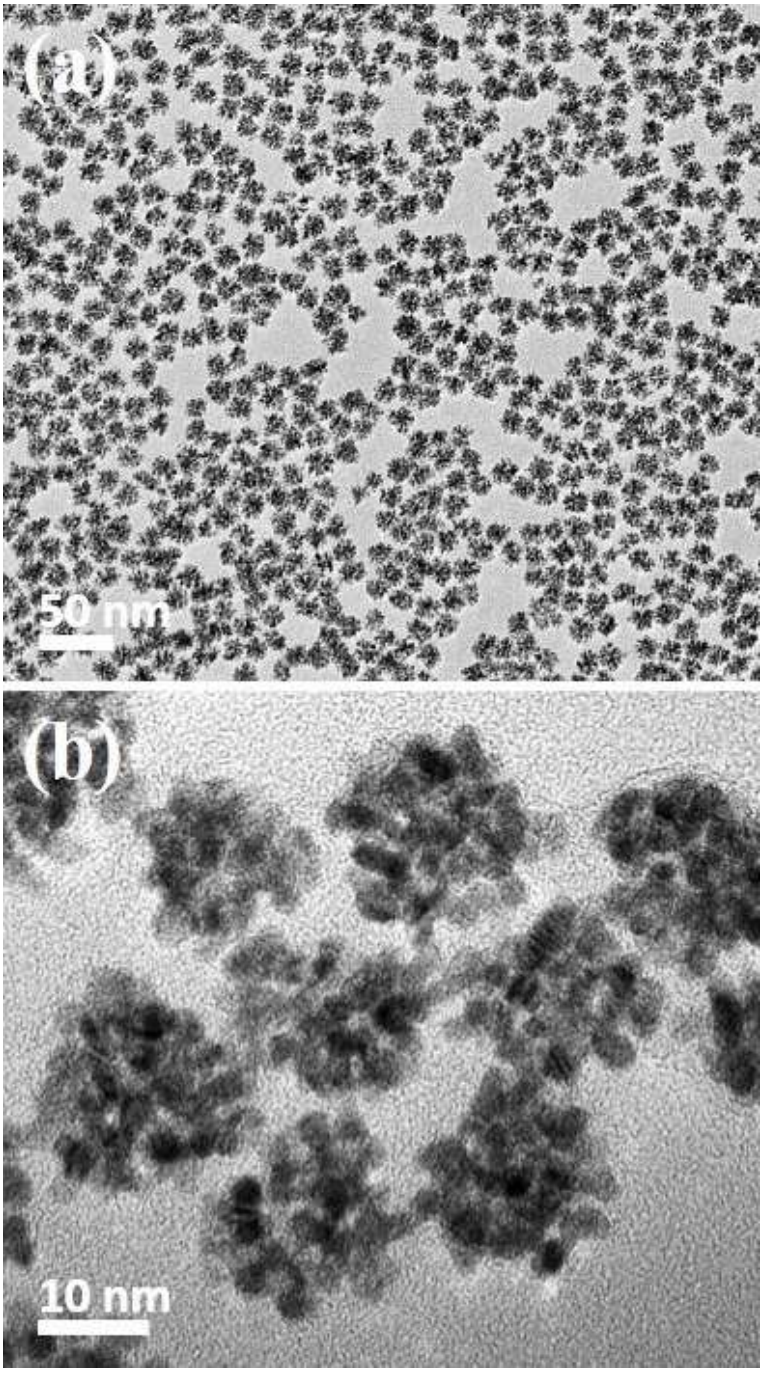

Figure 1. (a and b) TEM images of the porous PtCu NCs at different magnifications.

Nanoscale Accepted Manuscript

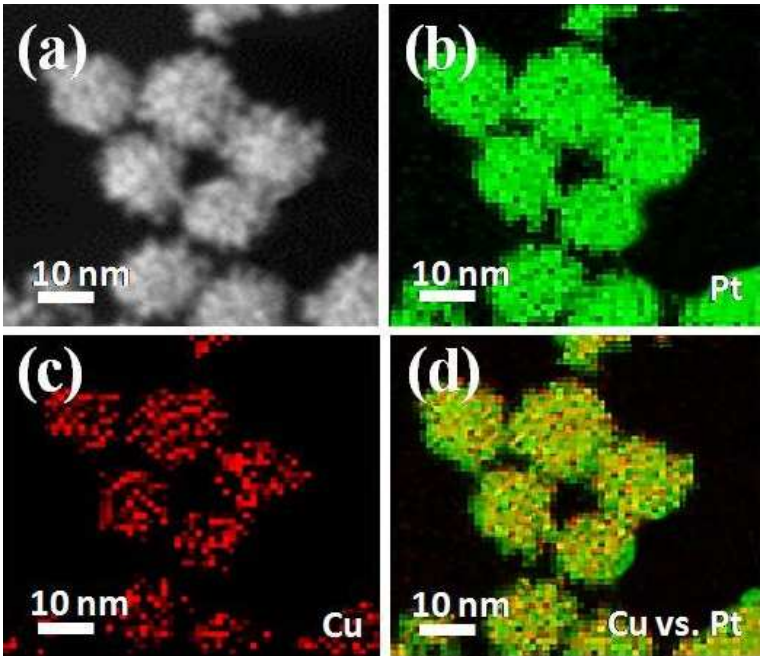

Figure 2. (a) HAADF-STEM and (b, c, and d) EDS elemental mapping images of the porous PtCu NCs.

Nanoscale Accepted Manuscript

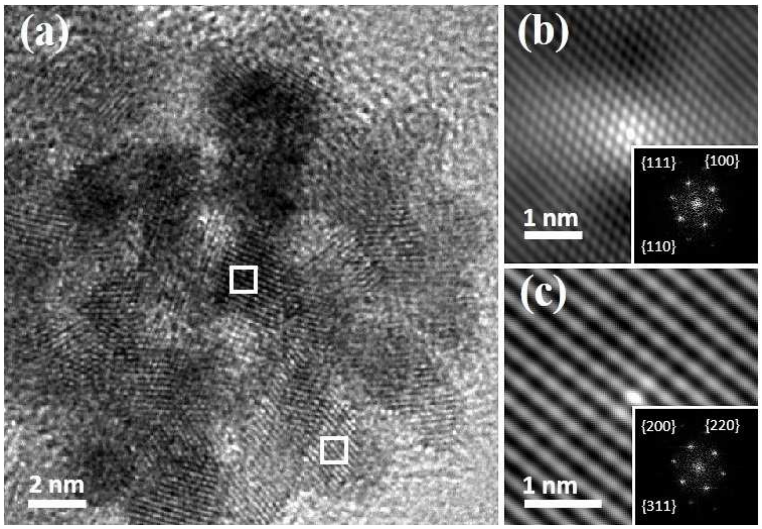

Figure 3. (a) Highly magnified TEM image of one porous PtCu NC. Fourier filtered lattice fringes in the core area (b) and in the shell area (c). The insets in (b) and (c) display the corresponding FFT patterns.

Nanoscale Accepted Manuscript

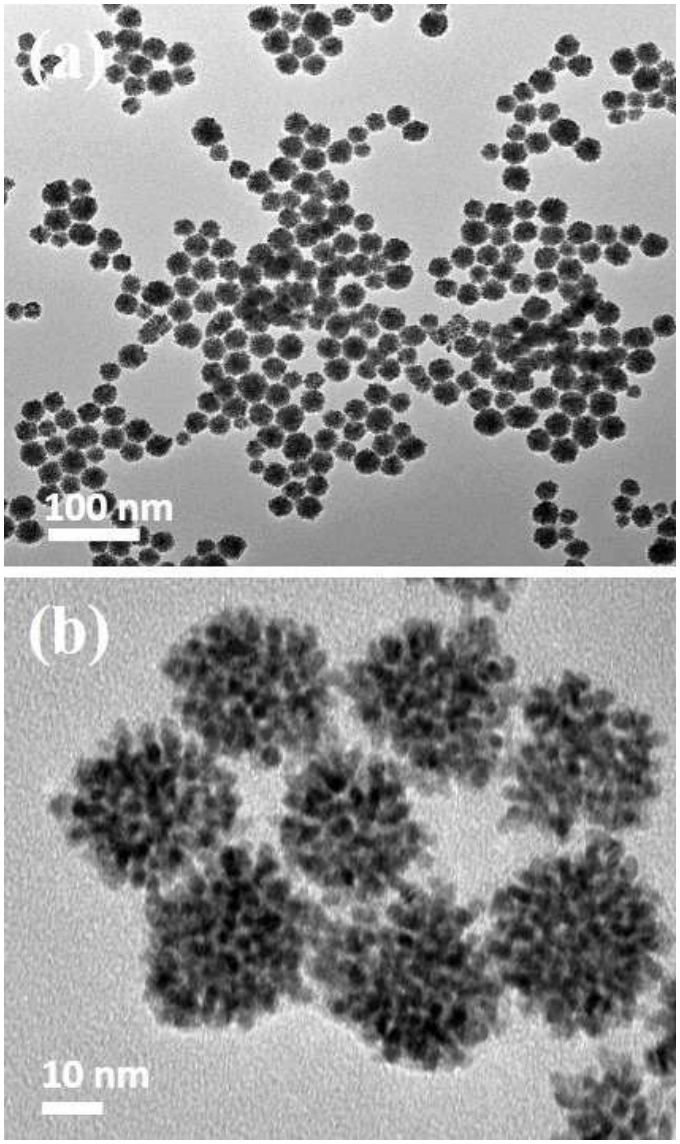

Figure 4. (a and b) TEM images of the dendritic PtCu NCs at different magnifications.

Nanoscale Accepted Manuscript

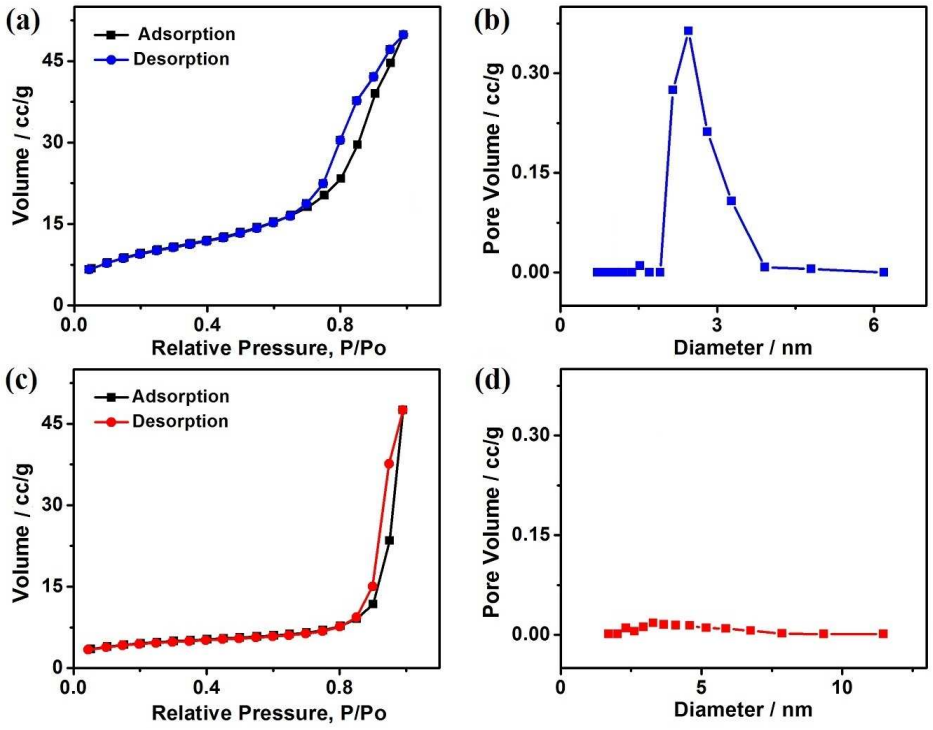

Figure 5. N_2 adsorption-desorption isotherms and pore-size distributions for porous PtCu NCs (a and b) and dendritic PtCu NCs (c and d).

Nanoscale Accepted Manuscript

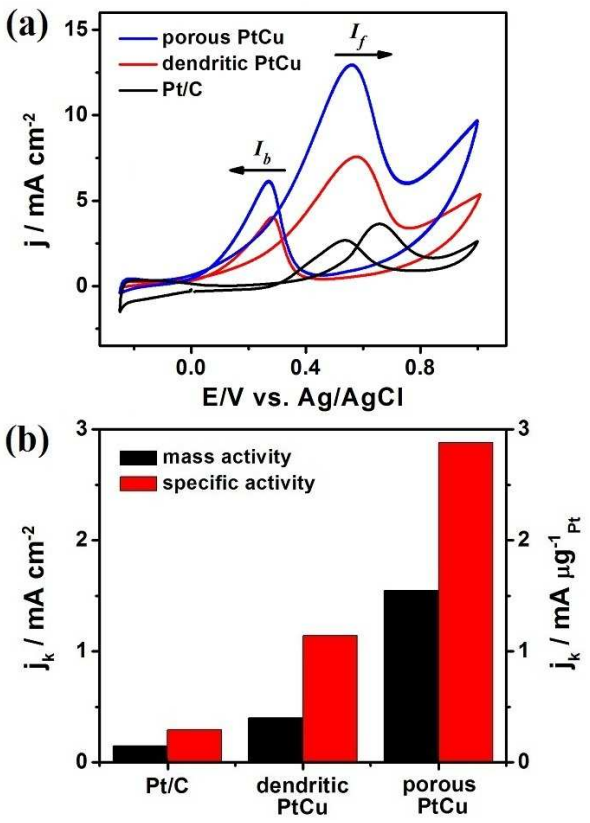

Figure 6. (a) CVs for MOR catalyzed by porous PtCu NCs, dendritic PtCu NCs, and Pt/C in 0.1 M $HClO_4$ with 1 M CH_3OH at a scan rate of 50 mV s^{-1}. (b) Comparisons of the mass and specific activities of the three materials.

Nanoscale Accepted Manuscript

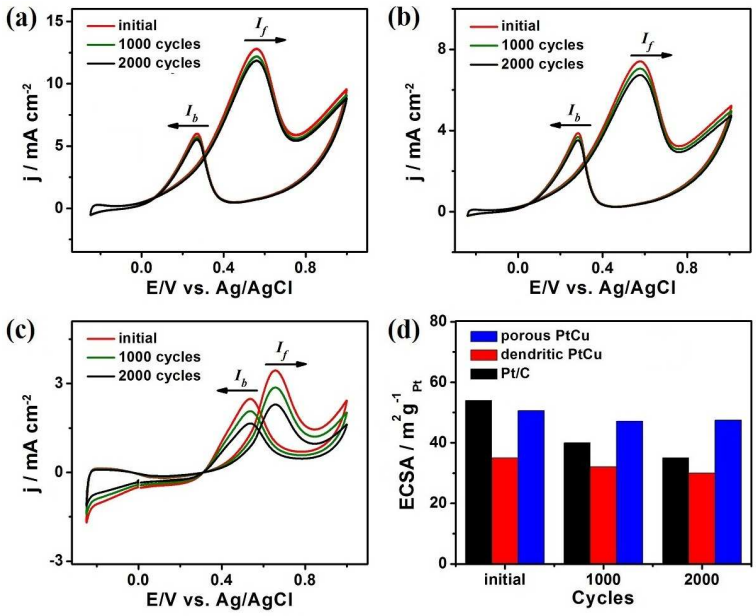

Figure 7. (a, b, and c) CVs for durability tests of the catalysts in 0.1 M $HClO_4$ with 1 M CH_3OH at a scan rate of 50 mV s^{-1}. (d) Comparisons of ECSAs of the catalysts.

Nanoscale Accepted Manuscript

Graphical Abstract

Porous bimetallic PtCu nanocrystals, which are highly active catalysts for the methanol oxidation reaction, are prepared by a one-step method.

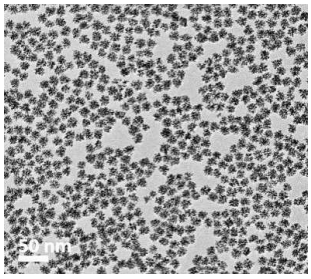

Nanoscale Accepted Manuscript